https://doi.org/10.5564/mjc.v23i49.1406
Mongolian Journal of Chemistry
www.mongoliajol.info/index.php/MJC

Efficiency of KOH-activated carbon for removal of heavy metal pollution from water

Narandalai Byamba-Ochir*, Nazgul Muratbyek, Narangarav Tumen-Ulzii, Ariunaa Alyeksandr, Nasantogtokh Oyunchimeg

Institute of Chemistry and Chemical Technology, Mongolian Academy of Sciences, Ulaanbaatar, 13330, Mongolia

** Corresponding author: narandalaib@mas.ac.mn;* ORCID ID: 0000-0002-2775-8984

Received: 4 November 2021; revised: 7 April 2022; accepted: 25 April 2022

ABSTRACT

The study to reduce heavy metals pollution from water using the KOH-activated carbon was studied the factors affecting the adsorption capacities of Cu (II) and Pb (II), in particular, initial metals concentration, pH of the solution, and contact time in static conditions. Using X-ray photoelectron spectroscopy and FTIR analysis to determine the elemental composition and surface functional groups of the activated carbon surface, the presence of oxygen-related functional groups was observed. The maximum adsorption capacities were 135.8 mg/g and 31.0 mg/g for removal of lead and copper solutions with the initial concentration of 300 mg/L of metal at 318 K, respectively. The removal percentage was found to be higher for Pb (II) when compared with Cu (II).

Keywords: KOH-activated carbon, heavy metals, surface characterization, adsorption isotherms

INTRODUCTION

Most heavy metals pollutants are released from metallurgical, oil refining, petrochemical, fertilizers/ pesticides production [1], electrochemical [2], leather and ceramic industries, and mining, particularly during gold mining activity of extracted ore [3]. These contaminants are a major cause of surface and groundwater pollution. The heavy metal pollutants are cadmium (Cd), chromium (Cr), mercury (Hg), nickel (Ni), lead (Pb), arsenic (As), copper (Cu), and zinc (Zn) are commonly associated with toxicity problems. Mining and metallurgical industries have been discharged toxic metals into the air, water and soil [4]. High levels of lead toxicity can lead to cognitive disorders, behavioral disorders, kidney damage and anemia [5]. Copper is relatively less toxic than lead, but excessive copper concentrations can lead to weakness, lethargy and anorexia, as well as damage to the gas-trointestinal tract [6].

In Mongolia, several studies have been investigated heavy metal pollution of groundwater, stream and soil around the mining industrial area, such as copper-molybdenum and gold mining factors [7-9]. Although heavy metals are often highly toxic, the recycling of some rare precious metals from contaminated waters is also a rationale for saving natural resources and protecting the environment [10]. At the same time, the removal of heavy metal pollutants from contaminated soil and natural water is an important task to prevent the ecosystem from severe environmental damage.

There are several methods for the removal of heavy metal pollutants from water media, in particular biological, chemical, and physical methods [11]. However, all of them have advantages and disadvantages, depending on their cost and disposal problems. Nowadays many techniques open up to remove these pollutants from water, such as chemical oxidation, coagulation, membrane separation, electrochemical and anaerobic microbial degradation, ion exchange, irradiation and adsorption. Among all of the methods adsorption has been allowed due to its cheapness and high quality of the treated wastewaters by well designated adsorption processes. Adsorption by activated carbon method is the most convenient method for regeneration after the removal process of pollutants. Its main advantage is the low operation cost of removal processes [12]. Furthermore, activated carbon is a well-known and popular adsorbent that has high porosity and a large surface area compared with other sorbent materials. Various pores with large surface area are dominant in

removing impurity molecules.

The adsorption method used by activated carbon is an integral part of alternative water purification methods, which allows for more economical cleanup opportunities. Because activated carbon is dense and resistant to chemical interactions, it is structurally less damaged when reused. Therefore, this study to conduct on the adsorption and separation of heavy metal ions from the aquatic media by natural coal derived activated carbons.

EXPERIMENTAL

Materials: The activated carbon (PMAC3) was prepared from semi-anthracite of the Tukhum deposit is located in East-Gobi of Mongolia by chemical activation with the mass ratio of activation agent (KOH) of 3:1 dry mixed directly in our previous study. Chemical activation was performed up to 400 °C with a heating rate of 5 °C/min for 2 h to remove volatile compounds and the temperature continuously increased to 750 °C and the sample powders were activated at 750 °C for 2 h [13].

The proximate and ultimate analyses of the initial sample were performed used with the Elemental analyzer (Flash 2000) are shown in Table 1.

Table 1. Proximate and ultimate analyses of the initial sample for the preparation of activated carbon

Proximate analysis (wt. %)				Ultimate analysis (wt. %)			
Fixed carbon	Volatiles	Ash	Moisture	C	H	N	Others
90.98	9.02	10.82	0.74	79.2	2.59	1.06	17.1

All chemical reagents ($Pb(NO_3)_2$, metal Cu, NaOH, HCl and HNO_3) used were analytical grade with 99.5% purity was used in all experimental studies. The reagent was purchased from Shanghai Macklin Biochemical Co.Ltd. The heavy metal solutions were prepared by dissolving the corresponding reagent in distilled water.

Equilibrium studies: All adsorption experiments were performed with 0.05 g activated carbon and 25 mL of heavy metal solutions with different initial concentrations (5 - 300 mg/L) in static conditions. The pH of the solution was adjusted with 1 mol/L HNO_3 or NaOH. The flasks with the sample were placed in an automatic shaker at a constant temperature (298, 308, and 318 K) and agitation speed of 150 rpm for 120 min. The samples were filtered after the adsorption process, and the residual concentration of metal ions was analyzed by UV-spectrophotometry and ICP-OES (Inductively coupled plasma - optical emission spectrometry).

The physical properties of activated carbons, such as the specific surface area, total pore volume, and pore size distributions were determined using N_2-adsorption data. The surface chemical property of activated carbons was analyzed by X-ray photoelectron spectroscopy (Multilab 2000, Thermoelectron Corp., England).

The removal of heavy metals using the activated carbons was carried out in static conditions and the factors affecting the adsorption capacities of KOH-activated carbon (PMAC3) for copper and lead were investigated in detail.

The adsorbed amount of metal ions q_t (mg/g) were calculated as follows:

$$q_t = \frac{(C_o - C_e) \cdot V}{m} \quad (1)$$

The heavy metals removal percentages were calculated as follows:

$$Removal, \% = 100\left(\frac{C_0 - C_e}{C_0}\right) \quad (2)$$

Where, C_0 and C_e (mg/L) are the initial and equilibrium concentration of the metal ion. V (L) is a volume of the metal solution, and m (g) is the mass of activated carbon [14, 15]. All adsorption data were optimized with the Langmuir, Freundlich, and Sips models to determine the effects of temperature and initial concentration.

Kinetic studies: Kinetic of metal ion adsorption was analyzed with an initial concentration of 100 mg/L at 298 K at different time intervals.

RESULTS AND DISCUSSIONS

Characterization of activated carbons: The detailed physical characterization results of the activated carbon sample are listed in Table 2. The anthracite based activated carbon (PMAC3) sample has a BET surface area of 2039 m^2/g.

Table 2. The physical properties of activated carbon

Texture parameters	Activated carbon
S_{BET}, m^2/g	2039
V_{micro}, cm^3/g	0.87
V_{meso}, cm^3/g	0.44
V_{total}, cm^3/g	1.31
D_{APD}, nm	1.97
DFT pore width (nm)	0.79
Bulk density (g/cm3)	0.33

The physical characteristics of activated carbon were estimated by the nitrogen adsorption and desorption data at 77 K using an adsorption analyzer (Micrometrics ASAP 2020, USA). The specific surface area (S_{BET}) of activated carbon was calculated by the Brunauer-Emmett-Teller (BET) method. The pore width was determined using the Density functional theory (DFT). The total pore volume (V_{total}), the micropore volume (V_{micro}), and the mesopore volume (V_{meso}) were estimated using Horvath & Kawazoe (HK) and the Barrett-Joyner-

Halenda (BJH) methods. The average pore size (D_{APD}) was calculated by expression: ($4V_t/S_{BET}$) using the BET surface area (S_{BET}) and total pore volume (V_t) from the BET [13] results.

The nitrogen adsorption and desorption isotherm curve and DFT pore size distribution of PMAC3 at 77 K are shown in Fig. 1. The nitrogen adsorption isotherm shows typical three steps with the increase in relative pressure. The first step is a steeply increasing region at low relative pressures less than 0.02, which stands for the adsorption or condensation in small micropores. Then the adsorption amount slowly increases with relative pressure without any notable hysteresis which represents the progressive filling of large micropores. Finally, the adsorption amount increases abruptly at near the saturation pressure of nitrogen because of active capillary condensation. The PMAC3 prepared in the study shows the type I isotherm according to the IUPAC classification in Fig. 1(a).

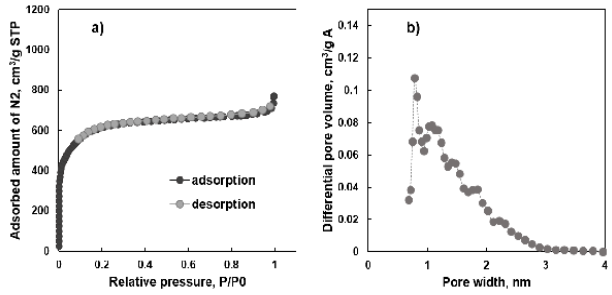

Fig. 1. Nitrogen adsorption/desorption isotherm and DFT pore size distribution of PMAC3

The activated carbon contains mostly micropores that have average pore diameters of 1.97 nm as shown in Table 2 and Fig. 1(b). For the activated carbon sample average DFT pore width was in the range of 0.79 nm [13].

When KOH-activation was used, small micropores seem to be well developed during activation since the chemical agent was more finely distributed inside anthracite particles than the simple physical mixing of KOH powder. PMAC3 sample prepared from semi- anthracite is highly porous with a wide range of micropores. As shown in Fig. 1(b), PMAC3 has properly developed mesopores of 1 - 2 nm.

The FTIR spectra of the RA and PMAC3 are shown in Fig. 2. The sample PMAC3 shows O-H stretching between 3300 - 3500 cm^{-1} like RA. In addition to this, C-H aliphatic stretching peak intensity is significantly increased at 2850 - 3000 cm^{-1} and 1300 - 1450 cm^{-1}. Similarly, C-O-C (stretching) phenolic deformation is found between 1000 - 1100 cm^{-1} with increased peak intensity.

Besides there are many small peaks of C=O, C-O is resolved to new lowest small peaks of carbonyl and carboxylic groups at 1639 - 1750 cm^{-1}, and C-H aliphatic bending peaks intensity is slightly increased at 1300 - 1450 cm^{-1}. It can be observed that the sample PMAC3 has much more contents of aliphatic C-H, carboxylic acid, and carbonyl groups (-C=O-).

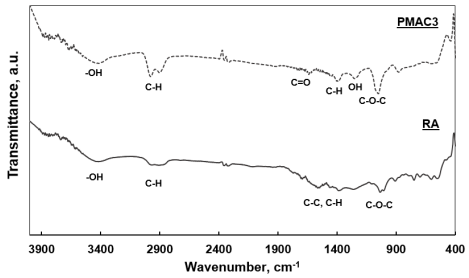

Fig. 2. FTIR spectra of RA and PMAC3

The chemical activation is responsible for the reasonably more oxygen functional groups in PMAC3. The surface hydrophilic nature of a material increases with surface oxygen bonded functional groups [16-19]. It can be suggested here that the sample PMAC3 has a slightly hydrophilic nature compared to that of RA according to this FTIR analysis. This suggestion was also confirmed by XPS analysis as discussed below.

The surface chemical properties of PMAC3 and raw anthracite (RA) samples were characterized by XPS analyses (Fig. 3 and Table 3).

Fig. 3 shows the C1 and O1 XPS spectral peaks of two samples, RA and PMAC3 for comparison. The surface elemental and high resolution C1s and O1s XPS spectra results of the samples are listed in Table 3, respectively.

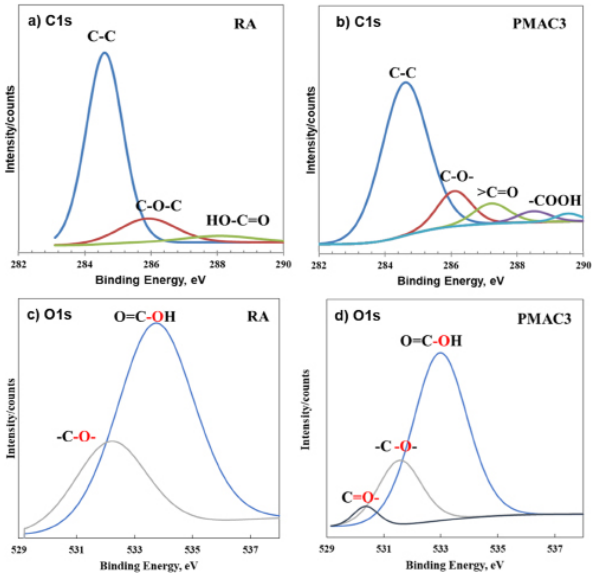

Fig. 3. High resolution C1s and O1s XPS spectral peaks of RA and PMAC3

From the Fig. 3, by the comparison of two samples, new oxygen bonded functional group (carbonyl) was created for PMAC3 after activation with KOH.

Table 3 listed typical XPS results of peaks together with fitted C1s and O1s spectrum.

Table 3. The surface functional groups of PMAC3 and RA (a resolution C1s and O1s)

The resolution	Peak	Functional group	Binding energy (eV)	Activated carbon (%, atomic)	
				RA	PMAC3
C1s	1	graphitic, aromatic (C-C)	284.6	79.39	74
	2	phenolic, alcoholic, etheric, (C-O-)	285.56-286.94	15.38	12.6
	3	carbonyl (C=O)	287.84-287.2	-	7.5
	4	Carboxyl (-COOH)	288.06-288.23	5.21	3.7
O1s	1	carbonyl (C=O)	530.4-531	-	7.35
	2	phenolic, alcoholic, etheric, (C-O-)	531.8-532.1	20.1	17.9
	3	Carboxyl (-COOH)	533	48.29	50.1
Cox/Cgr				0.259	0.322

Table 3 listed the binding energy (eV) and atomic percent of functional groups. From the comparison of the sample between raw anthracite and activated carbon, the C-C groups (graphitic and aromatic structure) of the resolution C1s was decreased after the activation process, while the carbonyl (C=O) group was extremely increased for activated carbon by examining XPS analysis. For this reason, the oxygen-bonded (carboxyl and carbonyl) groups on the surface of PMAC3 might be exhibit the relative activity for the lead and copper adsorption. Because the carboxyl groups and carbonyl groups play a significant role in metal ions adsorption, more surface adsorptive sites developed. Metallic ions (M+) might be retained in activated carbon by chemisorption involves the formation of surface complexes. It may be formed by ion exchange between H^+ and M^+ ions from the solution for carboxyl groups and by combination with the carbonyl groups. This can be done according to the following mechanism [2, 16]:

$$-C-COOH + M+ \rightarrow -C-COOM+ + H+$$
$$-C = O + M+ + H_2O \rightarrow -C-M\,(OH)_2$$

Equilibrium studies of adsorption

Effect of initial pH: Generally, the cationic heavy metal adsorption is based on the electrostatic interaction and ion exchange as an adsorption mechanism related to abundant the oxygen groups on the activated carbon surface, such as the hydroxyl and carboxyl groups. The −OH and −COOH groups on their surface can have different charges depending upon the pH of the solution [20].

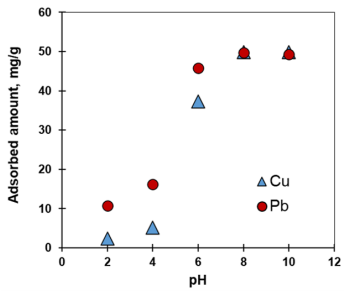

Fig. 4. The effect of pH on the metal ions adsorption

The pH of the initial solution is more effective on the adsorption capacity of the adsorbent. It is suggested that the ability to remove metal ions by adsorbent depends on the pH of the solution and this depends on the ion state and the surface properties of the adsorbent material. Fig. 4 shows the effect of pH on the metal ion adsorption capacity of copper and lead ions from aqueous solutions using the PMAC3 in a range of pH from 2 to 10.

The effect of pH on the Cu (II), and Pb (II) ions adsorption were studied at the temperature of 298 K, agitation speed of 150 rpm for the adsorption contact time required to reach the equilibrium was 120 min from metal ion initial concentration of 100 mg/L. In Fig. 4, the highest adsorbed amount of Cu (II), and Pb (II) ions were obtained at pH 8.0 and the lowest adsorbed amount was illustrated at pH 2.0. At high pH values, the activated carbon surface will convert to a more negative charge compared with low pH values. It might provide metal binding sites for ion exchange reaction and electrostatic interaction that are favorable to adsorb cationic species and high adsorption capacity.

In this way, carboxylic and carbonyl groups could provide additional ion binding capacity at pH 8.0.

Effect of adsorption temperature: The effect of adsorption temperature for adsorption of Cu (II), and Pb (II) ions onto PMAC3 were studied at the temperature of 298, 308 and 318 K, agitation speed of 150 rpm for the adsorption contact time required to reach the equilibrium was 120 min from the metal concentration of 300 mg/L. The adsorption isotherms of the copper and lead ions on the activated carbon sample are presented in Fig. 5. The adsorption isotherm data were optimized with the Langmuir, Freundlich and Sips isotherm models [21] due to well explain the adsorption mechanism of heavy metals.

The Langmuir isotherm expression is:

$$q_e = q_m \frac{K_L C_e}{1 + K_L C_e} \quad (3)$$

Where, C_e is the equilibrium concentration of metal ion (mg/L), q_e is the adsorption capacity (mg/g), K_L (L/mg) is the Langmuir isotherm constant, q_m signifies the theoretical monolayer capacity.

The key characteristics of the Langmuir isotherm have been described by the equilibrium constant (K_L), which is defined as:

$$K_L = 1/1+bC_0 \quad (4)$$

Where, C_0 is the initial concentration of metal ion, and *b* is the Langmuir constant.

The equilibrium constant (K_L) indicates the nature of adsorption [22] as:

$K_L > 1$ (unfavorable),
$0 < K_L < 1$ (favorable),
$K_L = 0$ (irreversible),
$K_L = 1$ (linear).

The Freundlich isotherm expression is:

$$q_e = K_F C_e^{1/n} \quad (5)$$

The Sips isotherms is given the following a general form:

$$q = \frac{q_m b C_e^{1/n}}{1 + b C_e^{1/n}} \quad (6)$$

where K_F (L/g) is the Freundlich isotherm constant, b is the Sips isotherm constant, *1/n* (dimensionless) is the heterogeneity factor [23].

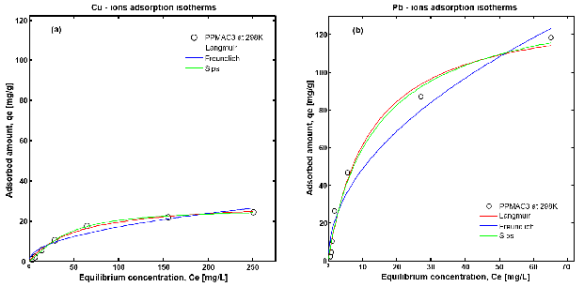

Fig. 5. (a) Cu-ions and (b) Pb-ions adsorption equilibrium isotherms data of the PMAC3 fitted with the Langmuir, Freundlich and Sips models

All isotherm models parameters and the correlation coefficient (R^2) are listed in Table 4. For the copper ions, adsorption data favorable isotherm was the Langmuir isotherm.

Because the Langmuir isotherm constant (K_L) is to be below 1.0. This result indicated the homogeneous adsorption of the activated carbon surfaces.

From the Table 4, comparing the values of q_m and R^2, the Sips isotherm predicted the lead ions adsorption data better than the Freundlich and the Langmuir isotherms. From the Sips isotherm model [20], the values of *1/n* attained were <1 for lead ions adsorption data, which suggests favorable adsorption behavior of lead ions on the activated carbon. The lead ions adsorption on the PMAC3 was found to follow the Sips isotherm model since the correlation coefficient, R^2 values obtained to best fit at all temperatures, in comparison to the Langmuir and the Freundlich isotherms where the values of R^2 were 0.99. The result suggested that heterogeneous adsorption for the lead adsorption data. The results showed that the most favorable isotherm was the Langmuir isotherm for Cu (II) ion adsorption onto PMAC3, but for adsorption of Pb (II) ions was the Sips isotherm. The maximum adsorption capacity was 31.9 mg/g for Cu (II) ion from the Langmuir isotherm model and 134.9 mg/g for Pb (II) from the Sips isotherm model with 300 mg/L of initial concentration of metal solution at 318 K as shown in Table 4.

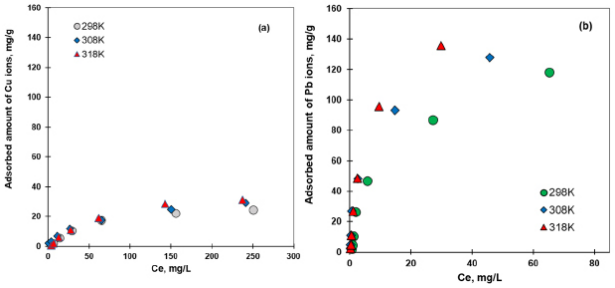

Fig. 6. (a) Cu (II) and (b) Pb (II) ions adsorption isotherms at different temperatures

The adsorption isotherms are illustrated in Fig. 6, which shows that the adsorbed amount of Cu (II) and Pb (II) ions increased with adsorption temperature. The increase in the adsorption amount of metal ions at high temperatures is due to the negative surface charge of the activated carbons and the adsorption process is endothermic. In other words, the results indicate that the ability of carboxyl groups involved in metal cations adsorption amount increased with the proton exchange adsorption mechanism.

Table 4. Adsorption isotherm parameters for Cu (II), Pb (II) ions on the ACs

Metal ions	Temp, K	Langmuir			Freundlich				Sips			
		q_{mm}	K_L	R^2	q_{mm}	K_F	1/n	R^2	q_{mm}	b	1/n	R^2
Cu (II)	298	28.7	0.02	0.99	30.0	1.86	0.48	0.94	27.9	0.007	1.33	0.99
	308	28.0	0.45	0.99	29.8	2.46	0.45	0.99	28.9	0.029	0.67	0.99
	318	31.9	0.01	0.99	33.8	1.72	0.54	0.96	31.3	0.007	1.24	0.99
Pb (II)	298	114.3	0.083	0.98	123.2	15.55	0.49	0.96	115.5	0.084	0.92	0.98
	308	122.3	0.201	0.98	133.9	26.42	0.42	0.96	126.1	0.184	0.79	0.99
	318	134.8	0.159	0.99	142.8	26.55	0.49	0.96	134.9	0.158	0.99	0.99

In Table 5, the results show that the removal efficiencies of PMAC3 for adsorption of Cu (II) and Pb (II) were 20.9% and 90.0% when the initial concentration of the metal solution of 300 mg/L at 318 K.

Table 4. The heavy metals adsorption capacity and removal efficiency percentage (at 300 mg/L of initial concentration of metals and 318 K

Adsorbent	Adsorbate	Adsorption capacity, mg/g	Efficiency, (%)
PMAC3	Cu (II)	31.9	20.9
	Pb (II)	134.9	90.0

Kinetic studies: The kinetic data were fitted with the pseudo-first-order and pseudo-second-order models [24, 25] for adsorption of Cu (II) and Pb (II) ions onto PMAC3. The correlation coefficient (R^2) is a fitting degree between experimental data and the model-predicted values. It can be assessed by which represents that the applied model is more feasible when this coefficient is close to or equal to 1.

In this work, the adsorption kinetic data were predicted with the Lagergren pseudo-first-order and pseudo-second-order models, which have been known as reliable models for a long time to describe the adsorption rate in batch adsorbers. The integrated linear form of the pseudo-first-order model can be expressed as follows [1, 24]:

$$\ln(q_e - q_t) = \ln q_e - K_1 t \quad (7)$$

where, q_e is the equilibrium adsorption capacity [mg/g], q_t is the adsorption capacity at time t [mg/g], and K_1 is the rate constant of the pseudo-first order adsorption (min^{-1}). Straight line plot of versus time confirms that the adsorption is governed by the first-order kinetics.

The pseudo-second-order model [25] can be expressed by a linear equation given below:

$$\frac{t}{q_t} = \left(\frac{1}{K_2 q_e^2}\right) + \frac{t}{q_e} \quad (8)$$

Where, K_2 (g/mg min) is the rate constant of the second-order adsorption.

The nonlinear forms of the above kinetic equations, which can be used to predict the adsorption equilibrium, as shown in equations 9 and 10:

$$q_t = q_e\left(1 - e^{-K_1 t}\right) \quad (9)$$

$$q_t = \frac{q_e^2 K_2 t}{(1 + q_e K_2 t)} \quad (10)$$

The rate constant of the second-order adsorption (K_2) and equilibrium adsorption capacity (q_e) are calculated from the intercept and slope of the plots of t / q_t versus t. The values of R^2 and q_e also indicate that these equations fitted well with experimental results as shown in Fig. 7 (a, and b). R^2 values for the pseudo-second-order kinetic model were found to be near 1 compared with the values of R^2 for the pseudo-first-order kinetic model.This indicates that the adsorption of metal ions on the PMAC3 obeys the pseudo-second-order kinetic model for the entire sorption period.

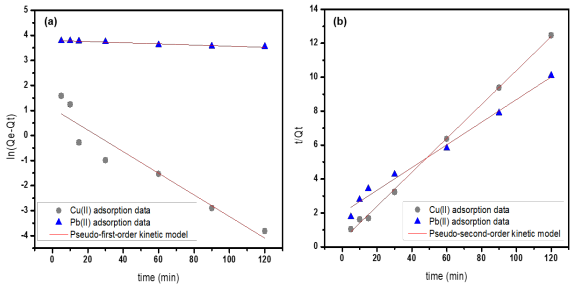

Fig. 7. Adsorption kinetics fitted with the pseudo first-order (a) and the pseudo-second order (b) model when the initial Cu (II) and Pb (II) ions concentration of 100 mg/L at 298 K.

The pseudo-first-order and pseudo-second-order kinetic models were used to investigate the kinetics as an important parameter for the adsorption mechanism and kinetics of the adsorption processes.

Table 4. The parameters of adsorption kinetic models of the PMAC3 at 298 K

Metal ion	Co (mg/L)	qe, exp (mg/g)	Pseudo-first-order			Pseudo-second-order		
			qe, cal (mg/g)	K_1 (1/h)	R^2	qe, cal (mg/g)	K_2 (g/mg h)	R^2
Cu (II)	61.800	4.765	4.775	1.244	0.99998	3.439	0.109	0.99849
	50.480	6.180	6.190	1.697	0.99983	4.943	0.065	0.99849
	28.789	8.885	8.553	2.203	0.99990	7.167	0.031	0.99849
	25.686	9.273	8.952	2.260	0.99993	8.242	0.029	0.99849
	24.460	9.431	8.945	2.269	0.99996	8.867	0.028	0.99849
	23.172	9.591	9.170	2.293	0.99997	9.195	0.027	0.99849
	22.906	9.625	9.272	2.296	0.99997	9.322	0.027	0.99849
Pb (II)	76.933	2.811	2.883	0.277	0.99962	1.321	0.063	0.98574
	75.767	2.955	3.667	0.706	0.99937	2.088	0.039	0.98574
	74.433	3.122	4.446	0.887	0.99880	2.759	0.026	0.98574
	63.267	4.516	7.092	1.383	0.98265	4.773	0.010	0.98574
	22.933	9.563	10.383	2.198	0.99956	7.661	0.005	0.98574
	8.172	11.408	11.479	2.395	0.99973	9.086	0.004	0.98574
	4.296	11.892	11.963	2.446	0.99980	9.914	0.004	0.98574

The adsorption amounts of Cu (II) and Pb (II) ions on PMAC3 were measured in terms of contact time. Fig.7 shows experimental data and predicted kinetic data from the pseudo-first-order (Fig.7(a)) and pseudo-second-order (Fig. 7(b)) models when 25 mL of 300 mg/L of metals was contacted with 0.2 g of the PMAC3 at 298 K.

The parameters of kinetic models are listed in Table 6. The correlation coefficients (R^2) for the pseudo-second-order model are slightly low, and the calculated qe values (qe, cal) from the pseudo-second-order model do not agree with the experimental data (qe, exp), suggesting that the Cu (II) and Pb (II) ions adsorption on the PMAC3 cannot be explained a pseudo-second-order model. However, the values of the correlation coefficient of the pseudo-first-order model (R^2 = 0.99) were much higher than pseudo-second-order model. On the other hand, the adsorption kinetics follows the pseudo- first-order equation, as shown in Fig. 7. Therefore, the adsorption kinetics were not suggesting a chemisorption process.

CONCLUSIONS

The KOH-activated carbon derived from semi-anthracite (PMAC3) for lead ions shows significantly higher adsorption capacities compared with copper ions adsorption. The lead removal efficiency of activated carbons was up to 90% within the 240 min, where the concentration of contact solution was 300 mg/L at 318 K. In fitting adsorption equilibrium data of heavy metal ions on the PMAC3, three isotherm equations, the Langmuir, Freundlich and Sips, were employed. Among them, the Langmuir isotherm was the most favorable isotherm for the copper ions adsorption data. This result indicated the homogeneous adsorption of the activated carbon surfaces. But for lead ions adsorption onto PMAC3 was found to follow the Sips isotherm model, the result suggested heterogeneous adsorption.

The copper and lead ions adsorption kinetic data of the PMAC3 were follow the pseudo-first-order equation, it suggesting that was not chemisorption process.

The KOH-activated carbon (PMAC3) with negative surface charge can be an effective candidate which is feasible adsorbent material for cationic heavy metal ions adsorption from aqueous media.

REFERENCES

1. Alcaraz L. García-Díaz I. Alguacil F.J. López F.A. (2019) Removal of copper ions in wastewater by adsorption onto a green adsorbent from winemaking wastes. Preprints, 2019090185. https://doi.org/10.20944/preprints201909.0185.v1
2. Gao X., Wu L., Xu Q., *et al*. (2018) Adsorption kinetics and mechanisms of copper ions on activated carbons derived from pinewood sawdust by fast H_3PO_4 activation. *Environ. Sci. Pollut. Res*., **25**, 7907-7915. https://doi.org/10.1007/s11356-017-1079-7
3. Fashola M.O., Ngole-Jeme V.M., Babalola O.O. (2016) Heavy metal pollution from gold mines: environmental effects and bacterial strategies for resistance. *Int. J. Environ. Res. Public Health*, **13**(11), 1047. https://doi.org/10.3390/ijerph13111047
4. O'Connell D.W., Birkinshawb C., O'Dwyer T.F. (2008) Heavy metal adsorbents prepared from the modification of cellulose: A review. *Bioresour. Technol.*, **9**(15), 6709-24. https:// doi.org/10.1016/j.biortech.2008.01.036
5. Pagliuca A., Mufti G.J., Baldwin D., et al. (1990) Lead poisoning: Clinical, biochemical, and haematological aspects of a recent outbreak. *J. Clin. Pathol.,* **43**(4), 277-281 https://doi.org/10.1136/jcp.43.4.277
6. Theophanides T., Anastassopoulou J. (2002) Copper and carcinogenesis. *Crit. Rev. Oncol. Hematol*., **42**(1), 57-64. https:// doi.org/10.1016/s1040-8428(02)00007-0
7. Jajinjav Yo, Bolormaa O, Ochirkhuyag B, Watanabe M, Prathumratana L, Kim K.W. (2019) Geochemical source and dispersion of copper, arsenic, lead, and zinc in the topsoil from the vicinity of Erdenet mining area, Mongolia. *Geochemistry: Exploration, Environment, Analysis*, **19**(2), 110-120 https://doi.org/10.1144/geochem2018-025
8. Battogtokh B, Lee J.M., Woo N. (2014) Contamination of water and soil by Erdenet copper-molybdenum mine in Mongolia. *Environmental Earth Sciences*, **71,** 3363-3374. https://doi.org/10.1007/s12665-013-2727-y
9. Azzaya T., Burmaa G., Alen S., *et al*. (2017) Arsenic occurrence in water bodies in Kharaa river basin. *Mongolian Journal of Chemistry*, **18**(44), 12-19. https://doi.org/10.5564/mjc.v18i44.932
10. Fu F., Qi Wang. (2011) Removal of heavy metal ions from wastewaters: A review. *Journal of Environmental Management,* **92,** 407-418. https://doi.org/10.1016/j.jenvman.2010.11.011
11. Rodríguez A., García H., Ovejero G, Mestanza M. (2009) Adsorption of anionic and cationic dyes on activated carbon from aqueous solutions: Equilibrium and kinetics. *Journal of Hazardous Materials,* **172**, 1311-1320. https://doi.org/10.1016/j.jhazmat.2009.07.138
12. Madani N., Bouchenafa-Saib N., Mohammedi O., *et al.* (2017) Removal of heavy metal ions by adsorption onto activated carbon prepared from Stipa tenacissima leaves. *Desalination and Water Treatment*, **64**, 179-188. https://doi.org/10.5004/dwt.2017.20254
13. Lee H.C., Byamba-Ochir N., Shim W.G., *et al*. (2015) High-performance super capacitors based on activated anthracite with controlled porosity. *Journal of Power Sources*, **275**, 668-674. https://doi.org/10.1016/j.jpowsour.2014.11.072

14. Egbosiuba T.C., Abdulkareem A.S., Tijani J.O. *et al*. (2020) Taguchi optimization design of diameter-controlled synthesis of multi walled carbon nanotubes for the adsorption of Pb(II) and Ni(II) from chemical industry wastewater, *Chemosphere*, **266**, 128937. https://doi.org/10.1016/j.chemosphere.2020.128937
15. Moreno-Castilla C., Álvarez-Merino M.A., Pastrana-Martínez L.M., López-Ramón M.V. (2010) Adsorption mechanisms of metal cations from water on an oxidized carbon surface. *Journal of Colloid and Interface Science*, **345**, 461-466. https://doi.org/10.1016/j.jcis.2010.01.062
16. Figueiredo J.L., Pereira M.F.R., Freitas M.M.A. and Orfao J.J.M. (1999) Modification of the surface chemistry of activated carbons. *Carbon*, **37**, 1379-1389. https://doi.org/10.1016/S0008-6223(98)00333-9
17. Yumitori S. (2000) Correlation of C1s chemical state intensities with the O1s intensity in the XPS analysis of anodically oxidized glass-like carbon samples. *Journal of Materials Science*, **35**, 139-146. https://doi.org/10.1023/A:1004761103919
18. Zhou J.H., Sui Z.J., Zhu J., Li P., Chen D., e*t al*. (2007) Characterization of surface oxygen complexes on carbon nanofibers by TPD, XPS and FT-IR. *Carbon*, **45**(4), 785-796. https://doi.org/10.1016/j.carbon.2006.11.019
19. Guixia Zhao, Xuemei Ren, Xing Gao, Xiaoli Tan, Jiaxing Li, *et al.* (2011) Removal of Pb(II) ions from aqueous solutions on few-layered graphene oxiden anosheets. *Dalton Trans*., **40**, 10945. https://doi.org/10.1039/C1DT11005E
20. Suresh Kumar, Rahul R. Nair, Premlal B. Pillai, *et al*. (2014) Graphene oxide-$MnFe_2O_4$ magnetic nanohybrids for efficient removal of lead and arsenic from water. *ACS Applied Materials & Interfaces,* **6,** 17426-17436. https://doi.org/10.1021/am504826q
21. Shou J., Qiu M. (2014) Adsorption of copper ions onto activated carbon from capsicum straw. *Desalination and Water Treatment*, **57**(1), 353-359. https://doi.org/10.1080/19443994.2014.966328
22. Attar K., Demey H., Bouazza D., Sastre A.M. (2019) Sorption and desorption studies of Pb(II) and Ni(II) from aqueous solutions by a new composite based on alginate and magadiite materials. *Polymers*, **11**, 340-358. https://doi.org/10.3390/polym11020340
23. Hall K.R., Eagleton L.C., Andreas Acrivos., Theodore Vermeulen. (1966) Pore- and solid-diffusion kinetics in fixed-bed adsorption under constant-pattern conditions. *Industrial & Engineering Chemistry Fundamentals*, **5**(2), 212-223. https://doi.org/10.1021/i160018a011
24. Huang Z., Liu S., Zhang B., *et al.* (2012) Equilibrium and kinetics studies on the absorption of Cu(II) from the aqueous phase using a β-cyclodextrin-based adsorbent. *Carbohydrate Polymers*, **88**(2), 609-617. https://doi.org/10.1016/j.carbpol.2012.01.009
25. Plazinski W., Dziuba J., Rudzinski W. (2013) Modeling of sorption kinetics: the pseudo-second order equation and the sorbate intraparticle diffusivity. *Adsorption*, **19**, 1055-1064. https://doi.org/10.1007/s10450-013-9529-0